The Cluster-Arranged Cooperative Model: A Model That Accounts for the Kinetics of Binding to A_1 Adenosine Receptors†

Rafael Franco, Vicent Casadó, Francisco Ciruela, Josepa Mallol, Carme Lluis, and Enric I. Canela*

Department of Biochemistry and Molecular Biology, Faculty of Chemistry, University of Barcelona, Martí i Franquès, 1, 08071-Barcelona, Catalonia, Spain

Received October 9, 1995; Revised Manuscript Received January 4, 1996⊗

ABSTRACT: To explain the equilibrium binding and binding kinetics of ligands to membrane receptors, a number of models have been proposed, none of which is able to adequately describe the experimental findings, in particular the apparent negative cooperativity of ligand binding. In this paper, a new model, *the cluster-arranged cooperative model*, is presented whose main characteristic is that it explains the existence of negative cooperativity in the binding of ligands to the receptor molecule. The model is based on our findings of agonist binding to A_1 adenosine receptors and of ligand-induced clustering of these receptors on the cell surface. The model assumes the existence of two conformational forms of the receptor in an equilibrium which depends on the concentration of the ligand. In this way, negative cooperativity is explained by the transmission of the information between receptor molecules through the structure of the membrane. The model is able to predict the thermodynamic binding and binding kinetics of [^{3}H]-(*R*)-(phenylisopropyl)adenosine to A_1 adenosine receptors in the presence and absence of guanylyl imidodiphosphate. In the presence of the guanine nucleotide analogue, the linear Scatchard plots obtained for [^{3}H]-(*R*)-(phenylisopropyl)adenosine binding are explained by the disappearance of cooperativity, thus suggesting that G proteins are important for the existence of negative cooperativity in ligand binding. Among other predictions, the model justifies early events in homologous desensitization since high ligand concentrations would lead to the saturation of the receptor in a low-affinity conformation that does not signal. Our model can likely explain the behavior of a number of heptaspanning and tyrosine-kinase receptors exhibiting complex binding kinetics.

Like other membrane receptors (De Meyts et al., 1978; Donner, 1980; Manger et al., 1981; Levitzki, 1981; Sibley et al., 1982; Neubig et al., 1988; Guijarro et al., 1989; Samama et al., 1993; Bond et al., 1995), A_1 adenosine receptors (Lohse et al., 1984; Klotz et al., 1986; Casadó et al., 1990a, 1993; Linden, 1991) apparently display two different affinity states, which depend upon the association between receptor and regulatory G protein. Thus, it is generally assumed that these receptors adapt to the *two independent receptors model*; i.e., they display two different affinity states that are independent because they are not kinetically interchangeable. It seems that the receptor coupled to the G protein exhibits high affinity for the agonist, whereas the uncoupled receptor shows low affinity. On the other hand, guanylyl imidodiphosphate [Gpp(NH)p], as well as other structural analogs of the GTP, promotes the conversion of the high-affinity state to the low-affinity state (Lohse et al., 1984; Linden, 1991; Allende et al., 1991). In contrast to that occurring in crude membranes, in the soluble extracts, obtained by treating crude membranes with a mixture of detergents, and in the detergent-treated membranes only the high-affinity state is detected (Casadó et al., 1990a). The distribution of the two affinity states varies in membranes with different microviscosity such as in myelin fractions (Casadó et al., 1991a, 1992). Modification of the ratio of the two affinity states has been induced by preincubating the crude membranes with either phospholipases (A_2, C, and D) or proteases (proteinase K, trypsin, and chymotrypsin) (Casadó et al., 1991b). These results suggested that the relative proportion of high- and low-affinity states depends upon the structure of the membrane.

Scatchard plots for binding, such as those obtained with adenosine receptor and other membrane receptors, correspond to Hill plots with a slope lower than 1. These Scatchard plots can result from a mixture of two or more affinity states or from negative cooperativity. We have strong kinetic evidence for negative cooperativity on the binding of [^{3}H]R-PIA to A_1 adenosine receptor from dissociation experiments at different ligand concentrations (Casadó et al., 1991c). The dissociation curves indicated that there is a ligand-induced transformation from high- to low-affinity states when high ligand concentrations are used. Obviously, this result cannot be explained by the *two independent receptors model*. This model cannot explain either the differences in maximum binding obtained when using different ligands (Allende et al., 1991) or the allosteric enhancement of binding caused by 2-amino-3-benzoylthiophenes (Bruns & Fergus, 1990).

In the present paper, we propose a model for the A_1 adenosine receptor that considers that each molecule of receptor affects the equilibrium and kinetic properties of other molecules, i.e., those included in the same membrane fragment or patch. This model is able to explain the thermodynamic and kinetic behavior of A_1 adenosine receptor. Moreover, this model would explain some aspects of ligand-induced desensitization of membrane receptors.

† This study was supported by Grants PB91-0263 and PB94-0941 from DGICYT.

* Author to whom correspondence should be addressed. Fax: 34-3-4021219. Phone: 34-3-4021208. E-Mail: r.franco@ub.es.

⊗ Abstract published in *Advance ACS Abstracts,* February 15, 1996.

0006-2960/96/0435-3007$12.00/0

EXPERIMENTAL PROCEDURES

Materials and Antibodies. [*Adenine*-2,8-^{3}H, *ethyl*-2-^{3}H]-N^6-(phenylisopropyl)adenosine ([^{3}H]R-PIA; 54 Ci/mmol) was purchased from New England Nuclear Research Products (Boston, MA); N^6-(*R*)-(phenylisopropyl)adenosine (R-PIA), guanylyl imidodiphosphate [Gpp(NH)p], and adenosine deaminase (EC 3.5.4.4) from Boehringer Mannheim (Germany); 50% (w/v) poly(ethylenimine) and crystallized serum albumin from Sigma Chemical Co. (St. Louis, MO). All other reagents were of the best grade available and purchased from Merk (Darmstadt, Germany). PC21 antibody is a polyclonal directed against an extracellular domain of the A_1 adenosine receptor; the characterization of this antibody has been described elsewhere (Ciruela et al., 1995). Mouse anti-rabbit IgG coupled to fluorescein isothiocyanate was purchased from Boehringer Mannheim. Deionized water, further purified with a Millipore Milli-Q system, was used throughout.

Immunofluorescence Analysis. DDT$_1$MF-2 cells were obtained from the American Type Culture Collection (Rockville, MO), which were cultured at 37 °C in 5% CO_2 using a Dulbecco's modified Eagle's medium (DMEM) supplemented with 5% fetal calf serum, 5% horse serum, 1% nonessential amino acids, 2 mM glutamine, and 1 mM sodium pyruvate. Cells grown on glass slides were incubated in the absence or presence of 50 nM R-PIA for 5 or 45 min. After being washed with phosphate-buffered saline, pH 7.4 (PBS), cells were fixed at 25 °C with freshly prepared 4% (w/v) paraformaldehyde in PBS for 15 min. After a wash with PBS containing 20 mM glycine, cells were treated for 15 min with 5% bovine serum albumin in PBS and then incubated for 60 min with 40 μg/mL PC21 antibody in the same medium. Three washes with 5% bovine serum albumin in PBS were performed before incubation with a mouse anti-rabbit IgG coupled to fluorescein isothiocyanate. Coverslips were washed in the same medium, mounted, and viewed through a Leica TCS 4D confocal scanning laser microscope. Photographic exposures were made using Kodak T-MAX 100 film.

Membrane Preparations. Porcine brains were obtained from the local slaughterhouse, and cortical membranes were prepared as described elsewhere (Casadó et al., 1990a,b). Cortices were dissected on ice and washed in 0.25 M sucrose containing 5 mM Tris-HCl buffer, pH 7.4. Tissue homogenization was performed in 10 volumes of the same buffer with a Polytron (Kinematica, PTA 20TS rotor, setting 4) for two periods of 5 s separated by an interval of 15 s. The addition of proteinase inhibitors to the homogenization medium did not improve the yield of receptor binding sites. The homogenate was centrifuged at 105000*g* for 30 min at 4 °C, and the pellet was washed twice by resuspension in 10 volumes of 50 mM Tris-HCl buffer, pH 7.4, and recentrifuged under the same conditions. The final pellet was suspended in the same buffer before use.

Protein Determination. Protein was measured by the method of Lowry et al. (1951) using bovine serum albumin as standard.

Radioligand Binding Experiments. Cortical membranes (0.6−0.75 mg of protein/mL) were incubated with adenosine deaminase (2 IU/mL) for 30 min at 25 °C in 50 mM Tris-HCl buffer, pH 7.4. Addition of [^{3}H]R-PIA prepared with the same buffer was then made. For kinetic experiments, 500 μL aliquots (3−5 replicates) were taken for filtration [Whatman GF/C filters presoaked in 0.3% poly(ethylenimine), 2−4 h, pH 10] at different time intervals. For equilibrium binding experiments, aliquots were taken after 4−8 h of incubation, which is enough time to achieve the equilibrium for each ligand concentration. Filters were subsequently washed in 10 mL of ice-cold 50 mM Tris-HCl buffer, pH 7.4, for <8 s. In all cases, the filters were incubated with 10 mL of Formula-989 cocktail (New England Nuclear Research Products) and shaked (12 h) at room temperature. Radioactivity of vials was counted using a Packard 1600 TRI-CARB scintillation counter with an efficiency of 57%.

Analysis of Kinetic Binding Data. Association−dissociation data were analyzed by nonlinear regression. A suitable program to fit data obtained from time course reactions (progress curves analysis; Canela & Franco, 1986) was used with the following equations (Casadó et al., 1990a,b, 1991c):

Association

$$R(\text{total binding}) = R_{\text{e slow}}(1 - e^{-tk_{\text{obs slow}}}) + R_{\text{e fast}}(1 - e^{-tk_{\text{obs fast}}}) + K_n[\text{L}] \quad (1)$$

Dissociation

$$R(\text{total binding}) = R_{\text{e slow}}e^{-tk_{-1\text{ slow}}} + R_{\text{e fast}}e^{-tk_{-1\text{ fast}}} + K_n[\text{L}] \quad (2)$$

In these equations, t is time, [L] represents free ligand concentration, $R_{\text{eq slow}}$ and $R_{\text{eq fast}}$ are the ligand bound at equilibrium to the slow and fast species, respectively, $k_{-1\text{ slow}}$ and $k_{-1\text{ fast}}$ are the dissociation rate constants for each species, and $k_{\text{obs slow}}$ and $k_{\text{obs fast}}$ are the association rate constants observed for each species: $k_{\text{obs}} = k_{-1} + k_{+1}[\text{L}]$, where the term k_- is the dissociation rate constant and k_+ is the association rate constant. $K_n[\text{L}]$ is the nonspecific binding, assuming that nonspecific apparent association and dissociation rate constants are very high and the nonspecific binding site concentration is much higher than the total ligand concentration (data not shown).

Analysis of Equilibrium Binding Data. Data were analyzed according to the models listed in Charts 1 and 2. The previously described programs for nonlinear regression (Canela, 1984; López-Cabrera et al., 1988; Canela et al., 1990) were used with the equations corresponding to each of the models analyzed. Goodness of fit was tested according to reduced χ^2 or SD values given by the programs. Models were compared using an F test as described by Munson and Rodbard (1980).

Simulation Procedure. Simulations using the differential equations corresponding to the model of Chart 2 were performed using a Gear's-based subroutine of the NAG library (D02EBF subroutine) which is useful to solve stiff differential equations.

RESULTS AND DISCUSSION

To demonstrate that the model presented (*cluster-arranged cooperative model*; see Chart 2) is able to explain the behavior of agonist binding to A_1 adenosine receptors, data from equilibrium binding and binding kinetic experiments were analyzed first with the classical *two independent receptors model* to establish and quantify the main discrepancies that appear in the results when this model is used, and, then, to the proposed model (Chart 2). Statistic-based

Chart 1

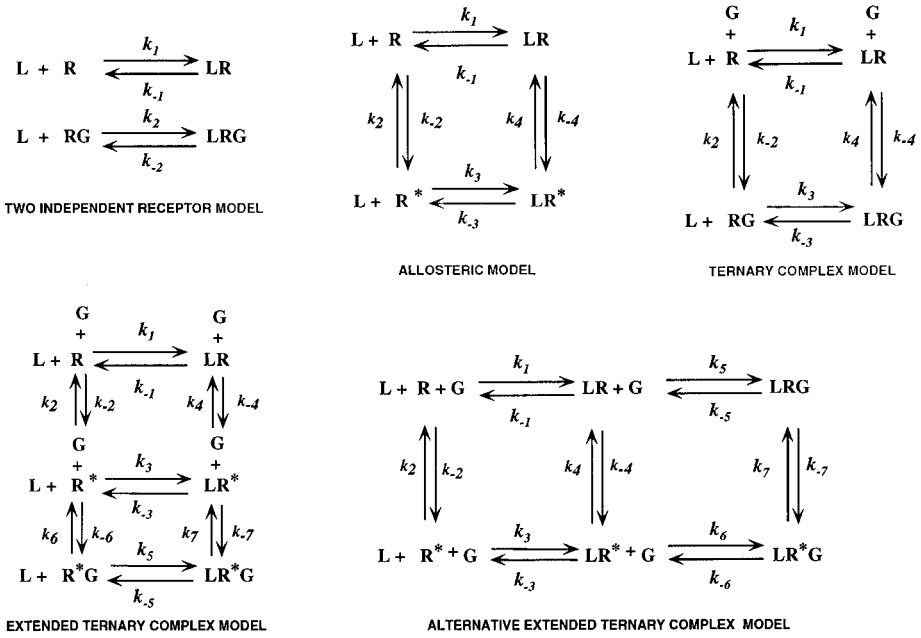

Chart 2: Cluster-Arranged Cooperative Model[a]

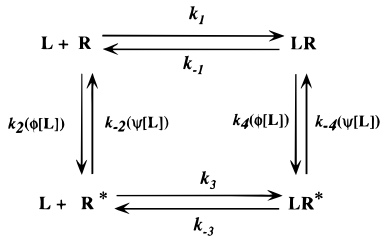

[a] k_2, k_{-2}, k_4, and k_{-4} values depend upon ligand concentration; see text.

tests have been used to compare the performance of the proposed model with other models (Chart 1): the *allosteric model* (Bruns & Fergus, 1990), the *ternary complex model* (De Lean et al., 1980), and the *extended ternary complex model* and the *alternative extended ternary complex model* (Samama et al., 1993) that results from a modification of the previous one.

Analysis of Binding Data with the Two Independent Receptors Model

Equilibrium Binding of [^{3}H]R-PIA. Studies of equilibrium binding of agonist [^{3}H]R-PIA were performed using a wide range of concentrations (between 0.05 and 19 nM) to define the binding parameters in the absence or presence of 100 μM Gpp(NH)p. As is well documented, the *two independent receptors model* explains the results by the existence of high- and low-affinity binding sites in absence of Gpp(NH)p (equilibrium parameters shown in Table 1) and by the existence of a single affinity state (R = 0.67 pmol/mg of protein and K_d = 2.9 nM) in the presence of the guanine nucleotide analogue.

[^{3}H]R-PIA Association and Dissociation Kinetics. Detailed studies of the time course of [^{3}H]R-PIA binding were performed over a 430-fold range of concentrations (0.05−19.34 nM) (Figure 1A). The time course of [^{3}H]R-PIA binding was fitted to two exponential phases (see Experimental Procedures). Semilogarithmic plots of specific binding *versus* time (0−25 min interval) are shown in Figure 1B. The semilogarithmic plots reveal that the fast component of binding increased steadily with ligand concentration (Figure 1B), whereas the slow component disappeared. The observed rate constants (k_{obs}) for the fast and slow phases of binding were plotted versus the free agonist concentration (Figure 2). The $k_{obs\ slow}$ increased linearly with R-PIA concentration until 0.8 nM (free ligand) (Figure 2A) and then linearity was lost (data not shown); $k_{obs\ fast}$ did not vary linearly with the R-PIA concentration (Figure 2B). These results are not consistent with a typical bimolecular reaction mechanism. In spite of the nonlinearity, a linear analysis of the data (see Figure 2A and straight line of Figure 2B) was performed according to the equation: $k_{obs} = k_{-1} + k_{+1}$[L]. The slope of the plot (the association rate constant) is $(1.31 \pm 0.09) \times 10^6$ M^{-1} s^{-1} for the fast phase of the binding and $(3.42 \pm 0.08) \times 10^5$ M^{-1} s^{-1} for the slow phase of the binding. The intercepts of the plot (the dissociation rate constants) for the fast and slow phases of binding are $(3.9 \pm 0.6) \times 10^{-3}$ s^{-1} and $(3.68 \pm 0.03) \times 10^{-4}$ s^{-1}, respectively. The equilibrium dissociation constants for the fast and slow phases calculated from the values of rate constants ($K_d = k_{-1}/k_{+1}$) are 3.02 nM and 1.08 nM, respectively. These estimates were similar to each other and also to that corresponding to the low-affinity component determined by equilibrium binding, but they differ from the value obtained for the high-affinity state (0.22 nM, see Table 1); this is a first indication of the inadequacy of the *two independent receptors model*. On the other hand, the binding at equilibrium of the slow phase (Figure 3A) increased to a maximum (0.8 nM free ligand; 1.1 nM total ligand). From this maximum, the binding at equilibrium decreased sharply, and at an agonist concentration of 8 nM and above, the slow phase was not detected, in agreement with the loss of linearity of the graph of rate constants *versus* R-PIA concentration (see above). In contrast, the binding at equilibrium of the fast phase (Figure 3B) increased with a dependence on R-PIA concentration that appeared to be hyperbolic and reached a value of 100% of the total binding.

[^{3}H]R-PIA bound at equilibrium (120 min at 25 °C) for a set of radiolabeled ligand concentrations (0.9, 4.5, 9.3, 18.2, and 28.4 nM) was dissociated by displacing with 300-fold nonlabeled R-PIA. Figure 1C shows that there were differ-

Table 1: Nonlinear Least-Squares Fitted Parameters for Two Independent Receptors Model and Cluster-Arranged Cooperative Model

	two independent receptor model[a]		
	without Gpp(NH)p	with 100 μM Gpp(NH)p[b]	cluster-arranged cooperative model[a,d]
kinetic parameters[c]			R_0 (pmol/mg of protein) 0.74 ± 0.02
$R_{eq\ slow}$ (pmol/mg of protein)	0.17 ± 0.03	0.06 ± 0.02	K_1 (nM) 4.8 ± 0.5
$k_{1\ slow}$ ($M^{-1}\cdot s^{-1}$)	$(5 \pm 1) \times 10^5$	$(4.2 \pm 0.4) \times 10^5$	k_1 ($M^{-1}\cdot s^{-1}$) $(1.2 \pm 0.1) \times 10^6$
$k_{-1\ slow}$ (s^{-1})	$(1.2 \pm 0.2) \times 10^{-4}$	$(1.1 \pm 0.2) \times 10^{-4}$	k_{-1} (s^{-1}) $(5.8 \pm 0.3) \times 10^{-3}$
$R_{eq\ fast}$ (pmol/mg of protein)	0.12 ± 0.03	0.09 ± 0.02	K_{20} 0.60 ± 0.08
$k_{1\ fast}$ ($M^{-1}\cdot s^{-1}$)	$(3.3 \pm 0.5) \times 10^6$	$(3.8 \pm 0.3) \times 10^6$	k_{20} (s^{-1}) $(9.3 \pm 0.2) \times 10^{-2}$
$k_{-1\ fast}$ (s^{-1})	$(4.0 \pm 0.4) \times 10^{-3}$	$(4.7 \pm 0.5) \times 10^{-3}$	k_{-20} (s^{-1}) $(5.7 \pm 0.3) \times 10^{-2}$
equilibrium binding parameters[c]			K_3 (nM) 0.50 ± 0.03
R_0 ($R_{high} + R_{low}$) (pmol/mg of protein)	0.69 ± 0.02	0.67 ± 0.09	k_3 ($M^{-1}\cdot s^{-1}$) $(4.4 \pm 0.4) \times 10^5$
R_{high} (pmol/mg of protein)	0.29 ± 0.06		k_{-3} (s^{-1}) $(2.2 \pm 0.2) \times 10^{-4}$
$K_{d\ high}$ (nM)	0.22 ± 0.05		k_{40} (s^{-1}) $(3.6 \pm 0.3) \times 10^{-11}$
R_{low} (pmol/mg of protein)	0.4 ± 0.1	0.7 ± 0.2	k_{-40} (s^{-1}) $(2.0 \pm 0.1) \times 10^{-12}$
$K_{d\ low}$ (nM)	4.9 ± 0.5	2.9 ± 0.4	Y $(7.0 \pm 2.0) \times 10^{-2}$
			f 1.2 ± 0.2

[a] Definitions of the models are in Charts 1 and 2. [b] Membranes were incubated (30 min, 25 °C) with 100 μM Gpp(NH)p prior to [^{3}H]R-PIA addition. [c] Experimental details and data are given in Figure 1 and under Experimental Procedures. [d] Experimental data are given in Figure 1.

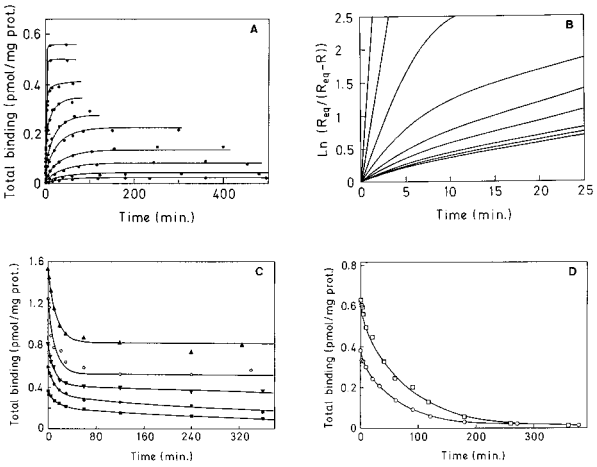

FIGURE 1: [^{3}H]R-PIA association and dissociation kinetics. R_{eq} represents specific binding at equilibrium, and R is specific binding at the indicated time. All experiments (of either association or dissociation) were performed in the same session with the same preparation of brain membranes. Panel A shows the association kinetic curves which were performed using the following [^{3}H]R-PIA concentrations (bottom to top): 0.05, 0.09, 0.18, 0.33, 0.71, 1.11, 2.25, 4.38, 8.83, and 19.34 nM. In panel B, the semilogarithmic plot of the first 25 min (derived from panel A) is displayed. In panel C, the dissociation kinetics of [^{3}H]R-PIA binding (■, 0.9; ●, 4.5; ▼, 9.3; ○, 18.2; and ▲, 28.4 nM) displaced after 2 h incubation at 25 °C using 300-fold unlabeled R-PIA are shown. Experiments of the displacement of [^{3}H]R-PIA (○, 1 and □, 17 nM) by dilution are shown in panel D. The procedure after incubation for 2 h at 25 °C was as follows: the sample was centrifuged at 105000*g* for 30 min at 4 °C, and dissociation was induced by dilution of the pellet to 0.030−0.037 mg of protein/mL. At different time intervals, 10 mL aliquots (3−5 replicates) were taken for filtration and subsequent analysis. Data were fitted, by nonlinear regression (Casadó et al., 1990a,b, 1991a; Canela & Franco, 1986), to *two-exponential phases model* according to the equations described under Experimental Procedures.

ences in dissociation kinetics for the various ligand concentrations. So, biphasic kinetics were observed for low ligand concentrations and monophasic kinetics for high ligand concentrations, and, as occurred in association kinetic experiments, in these experiments the slow phase of the dissociation disappeared at high ligand concentration. In fact, the percentage of the slow phase component diminished from 53% at 0.9 nM ligand concentration to 25% at 9.3 nM and to 0% at ligand concentrations equal or higher than 18.2 nM. In contrast, when similar experiments were carried out by dilution, biphasic curves were always obtained (Figure 1D).

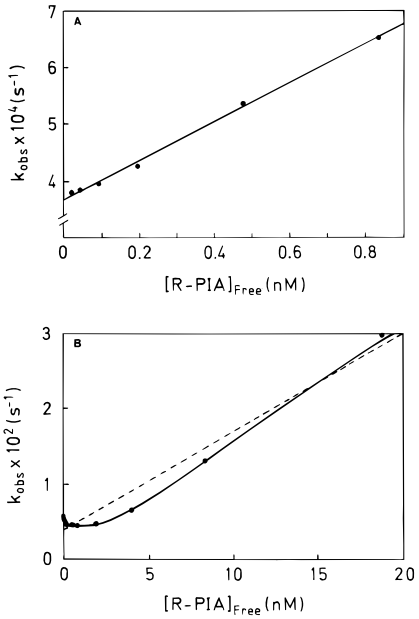

FIGURE 2: Dependence of rate constants of [^{3}H]R-PIA association kinetics on ligand concentration. Plots show the rate constant (k_{obs}) of the slow phase (A) and of the fast phase (B) *versus* free [^{3}H]R-PIA concentration. Values were determined from the results of nonlinear least-squares analysis of association kinetics as illustrated in Figure 1.

[^{3}H]R-PIA Binding Kinetics in the Presence of Gpp(NH)p. The time course of 1 nM [^{3}H]R-PIA binding in the absence or presence of 100 μM Gpp(NH)p was performed. In both cases, two phases for association and dissociation plots were observed whose parameter values appear in Table 1. The kinetic constants are similar in both cases, whereas the binding at equilibrium decreases markedly due to a slight reduction in $R_{e\ fast}$ and a notable reduction in $R_{e\ slow}$. There is a surprising discrepancy of these data with equilibrium binding data which indicates a unique affinity state in the presence of 100 μM Gpp(NH)p with a K_d of 2.9 nM (see above).

Conclusions about the Inadequacy of the Two Independent Receptors Model and Other Previously Described Models. The allosteric model (see Chart 1) cannot account for the results presented since it always leads to a hyperbolic binding isotherm (linear Scatchard plot). A nonhyperbolic binding isotherm can be obtained from (a) ligand binding to two (or more) different receptors operating independently, from (b)

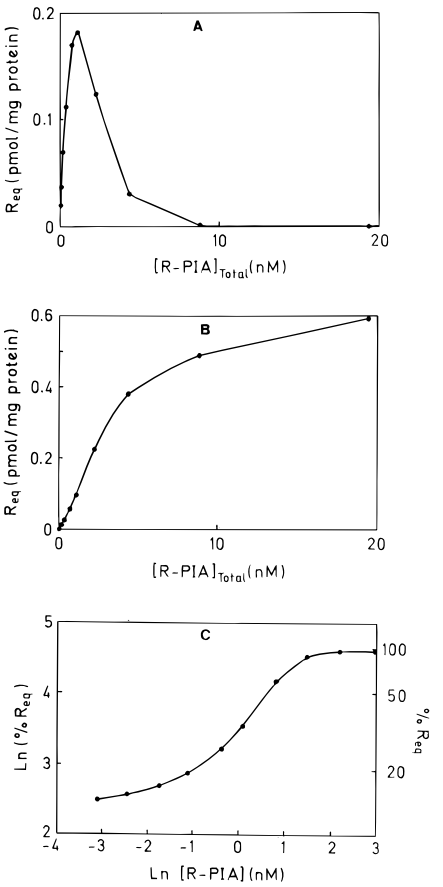

FIGURE 3: Dependence of binding at equilibrium on [^{3}H]R-PIA concentration. Plots show the binding at equilibrium for the slow phase (A) and the binding at equilibrium for the fast phase (B) *versus* free [^{3}H]R-PIA concentration. (C) is the double neperian logarithm plot of the percent of binding at equilibrium occurring during the fast phase *versus* free [^{3}H]R-PIA concentration (the right axis shows the percent of binding at equilibrium for the fast phase). Values were determined from the results of nonlinear least-squares analysis of association kinetics as illustrated in Figure 1A.

ligand binding to a unique type of receptor exhibiting cooperativity (not shown in Chart 1), or from (c) ligand binding to receptor to which, in addition to the binding of ligand, another different molecule such as, for instance, the G protein binds (G protein cannot be in great excess because otherwise the isotherm would be hyperbolic). Obviously, the combination of two of these possibilities would also lead to nonhyperbolic behavior. The fact that the slow component in association and dissociation kinetic experiments disappears at high ligand concentration totally rules out the possibility of a system formed by independent receptors, i.e., the classical *two independent receptors model*. Moreover, the hypothesis that the binding of G protein can explain the behavior of A_1 receptors should be ruled out since a single model based on this fact such as, for instance, the *ternary complex model* could justify a relative reduction of one of the components of the binding but not its complete disappearance. Also, it should be noted that a unique type of receptor exhibiting cooperativity due to an allosteric site or to the interaction of few subunits could not explain the drastic change of association and dissociation kinetics found when Gpp(NH)p is included in the assays. The set of results can only be accommodated by using a model permitting negative cooperativity. For receptors (or enzymes) in solution, the negative cooperativity is explained by the existence of oligomeric proteins. However, for membrane receptors, there is a model that can explain negative cooperativity in ligand binding without assuming the existence of oligomers, although without discarding them. This is the *cluster-arranged cooperative model* described below.

Derivation and Analysis of the Cluster-Arranged Cooperative Model

The Cluster-Arranged Cooperative Model Accounts for the Kinetics and Equilibrium Properties of the A_1 Adenosine Receptor. In order to explain the negative cooperativity found in ligand binding, our model assumes that cooperativity is due to a general interaction between a wide set of receptor molecules, not necessarily in direct contact but communicated through the different components of the membrane. Ligand binding to a receptor molecule would produce an alteration of the membrane sufficient to modify the rate constant for association of another ligand molecule to a second receptor molecule not necessarily located in the close neighborhood. In this way, the rate constants for the subsequent associations and dissociations would be sequentially modified.

Under physiological conditions, integral membrane proteins are free to diffuse laterally in the membrane, and, in the case of single-pass transmembrane receptors, the hormone produces a change in the oligomeric state of the receptor [see Wells (1994) for a review]. This oligomerization has not been described for heptaspanning receptors, but in Figure 4 we present evidence that the distribution of A_1 receptor molecules, detected by immunofluorescence on the DDT_1-MF-2 cells, is homogeneous in the absence of R-PIA, whereas in its presence they form clusters. Clustering, which is already evident after 5 min of treatment with R-PIA (Figure 4b,c), is maintained after prolonged incubation (45 min) with the agonist (data not shown). Since the A_1 adenosine receptor of DDT_1MF-2 cells has the same kinetic behavior as the pig brain receptor described here (data not shown), the *cluster-arranged cooperative model* (shown in Chart 2) can be based upon the hypothesis that receptor molecules are homogeneously distributed in the absence of the ligand whereas in its presence they aggregate. When a molecule of ligand binds to a molecule of receptor, it is highly probable that kinetic and equilibrium constants for the conformational change R (or RL) $\leftrightarrows$ R* (or R*L), which converts the low-affinity state form (R) into the high-affinity state form (R*) of the receptor, are modified. The explanation of the behavior of the system in the presence of Gpp(NH)p (Table 1) is that the cooperativity is lost, thus indicating that G proteins are essential for the cooperativity phenomenon in this system. In this particular case, the model is indistinguishable from the *allosteric model*. When cooperativity is prevented by the use of Gpp(NH)p, our model predicts two components in kinetic experiments. Consequently, the existence of two forms of the receptor in the absence and in the presence of Gpp(NH)p would indicate that both R and R* in our model (Chart 2) correspond to two conformational receptor−G protein complexes. Another model, similar to that presented in Chart 2 but including a further equilibrium corresponding to the uncoupled receptor form (uncoupled from G protein), could be considered, but it would not result in a significant improvement in performance. However, it should be taken into account that in this extended model, the rate constants for the new equilibrium should be indistinguishable from those of the low component of the binding in the *cluster-arranged cooperative model*; otherwise, one single component of the binding in

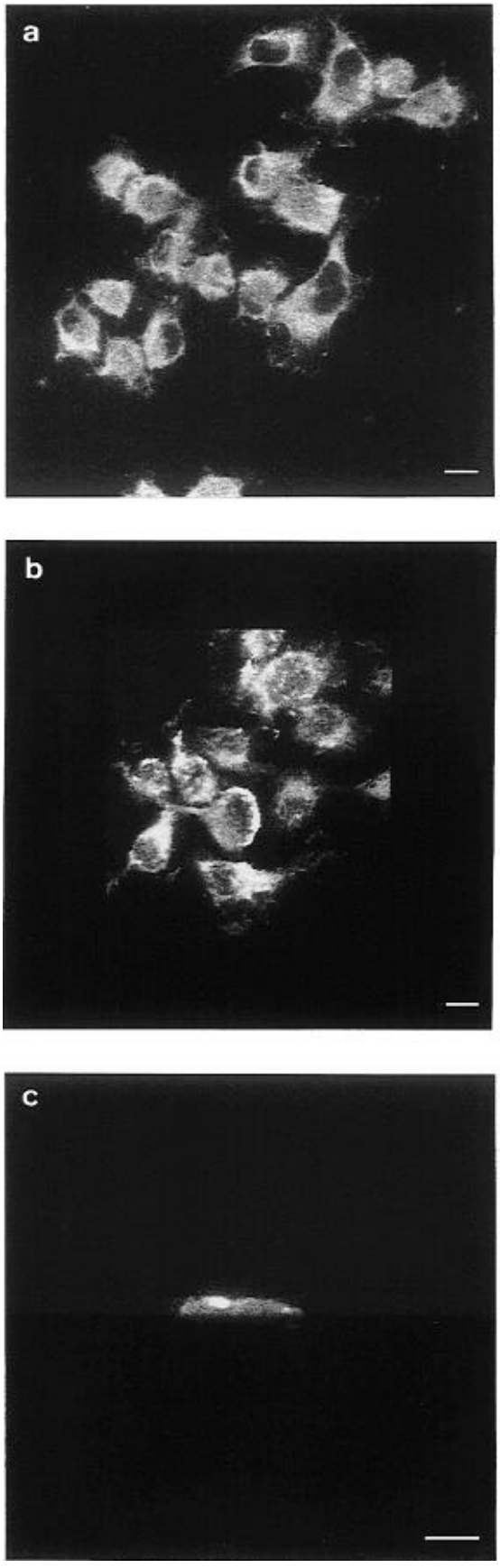

FIGURE 4: Immunofluorescence detection of A_1 adenosine receptors in DDT_1MF-2 cells. PC21 antibody was used to stain control cells (a) or cells treated with 50 nM R-PIA for 5 min (b). Panel c: Image corresponding to a vertical section of a single cell from (b). Scale bar: 10 μm.

association−dissociation experiments in the absence of Gpp(NH)p would never be obtained.

The equation describing the equilibrium binding of the model in Chart 2 can be written as

$$\text{total binding} = \frac{R_0 L}{L + [K_1K_3(1 + K_2)/(K_3K_2 + K_1)]} \quad (3)$$

where R_0 is the maximum equilibrium binding and stands for $R + R^* + RL + R^*L$, and K_1, K_3, and K_2 are defined as

$$K_1 = \frac{k_{-1}}{k_1} \quad (4)$$

$$K_3 = \frac{k_{-3}}{k_3} \quad (5)$$

$$K_2 = \frac{k_{-2}}{k_2} = \frac{k_{-20}(1/Y)^{zf}}{k_{20}(1/Y)^{z(f-1)}} = K_{20}(1/Y)^z \quad (6)$$

k_2 and k_{-2} are not true rate constants; they are only the rate *constant* for a given degree of occupancy of the receptor for the conversion of R* into R and *vice versa*, respectively. The true rate constants are k_{20} and k_{-20}, which are defined when the degree of occupancy of the receptor is zero. Similarly, K_{20} is the true equilibrium constant, whereas K_2 is a apparent one.

The parameter Y represents the cooperativity, and f denotes a dimensionless microscopic factor tailoring the different responses of forward and backward rate constants, whereas z is a variable that measures the degree of occupancy of the receptor:

$$z = \frac{\text{bound receptor}}{\text{free receptor}} \quad (7)$$

It should be noted that z varies between 0 and infinity. According to the proposed model, a value of Y less than 1 signifies that the increment of ligand bound to the receptor favors the transformation of R* (or R*L) into R (or RL).

As shown in the above equations and in Chart 2, K_1 and K_3 represent the affinity of R and R*, respectively. The equilibrium constant for the transformation of RL* into RL, K_4, which does not appear in the equation, can be substituted by a combination of K_1, K_2, and K_3. In fact, since the overall free energy necessary to convert R into R*L must be independent of the path taken, the value of K_4 can be determined from the values of the other equilibrium constants according to the equation

$$K_1K_4 = K_2K_3 \quad (8)$$

Actually, K_4 is defined as

$$K_4 = \frac{k_{-4}}{k_4} = \frac{k_{-40}(1/Y)^{zf}}{k_{40}(1/Y)^{z(f-1)}} = K_{40}(1/Y)^z \quad (9)$$

As above, K_4, k_4, and k_{-4} are not true constants. Their meaning, according to Chart 2, is similar to that of K_2, k_2, and k_{-2}. It should be noted that K_2 and K_4 are independent of f (see eqs 6 and 9).

For this model, total binding as a function of ligand concentration (eq 3) cannot be represented by an analytically-solvable equation due to the fact that z depends on the degree of occupancy of the receptor; i.e., it is a function of the ligand bound. For this reason, the plot of ligand bound *versus* free

ligand is not a hyperbole. On defining K_{app} as

$$K_{app} = \frac{K_1K_3[1 + K_{20}(1/Y)^z]}{K_3K_{20}(1/Y)^z + K_1} \quad (10)$$

and assuming that Y is less than 1 (that is, there is negative cooperativity), we can deduce that the limit of K_{app} as z tends to 0 is

$$K_{app} = \frac{K_1K_3(1 + K_{20})}{K_3K_{20} + K_1} \quad (11)$$

whereas as z tends to infinity the limit is

$$K_{app} = K_1 \quad (12)$$

Thus, our model predicts that models which do not take into account this variation of K_{app} with the receptor occupancy (e.g., the two independent receptor model) will give different values for the equilibrium constant when calculated from equilibrium binding data or from kinetic data.

Nonlinear Least-Squares Analysis of [^{3}H]R-PIA Equilibrium Binding. Equilibrium binding data obtained in the absence or presence of Gpp(NH)p have been fitted to suitable equations for the different models in Chart 1 and 2. The residual sum of squares of the fit to the different models was identical except in the case of the *allosteric model*, which was greater. As an example, we show, in Table 1, the results of the fit to the *cluster-arranged cooperative model* (Chart 2) and to the *two independent receptor model* (Chart 1). The only parameter that can be directly compared is the maximum binding (R_0), which is higher in the *cluster-arranged cooperative model*. With the experimental limitations, the *two independent receptors model* would, in statistical tests, be always selected as the simplest model able to explain the experimental isotherm. This indicates that discrimination between these two models and the other models of Chart 1 can only be achieved at higher ligand concentrations, i.e., at concentrations giving practical saturation of the receptor. In the case of adenosine receptors, this is not possible with the standard experimental procedures. However, it has been demonstrated by simulation that the magnitude of the differences of R_0 depends upon the value of Y; the greater its value, the greater the differences between models (data not shown). From K_1 and K_3 values, it can be deduced that R is the low-affinity form and R* is the high-affinity receptor.

Nonlinear Least-Squares Analysis of [^{3}H]R-PIA Binding Kinetics. The results of association experiments were analyzed according to the *cluster-arranged cooperative model*. The number of independent kinetic parameters was 10 including the receptor concentration. Despite the fact that the *two independent receptors model* cannot explain the results, the data were also fitted to this model for statistical comparison. In this case, the number of independent kinetic parameters was 5 (Table 1). The *cluster-arranged cooperative model* gave the best fit [$P < 0.01$ according to the F test as described by Munson and Rodbard (1980)]. From the values shown in Table 1, it becomes evident that the association and dissociation processes for the low-affinity form of the receptor occur faster than those for the high-affinity form ($k_1 > k_3$ and $k_{-1} > k_{-3}$). On the other hand, interconversion between empty R and empty R* is faster than the interconversion between the filled forms. The value of Y indicates a high degree of negative cooperativity (a value of 1 would imply absence of cooperativity). The value of f greater than 1 indicates that both k_2 (also k_4) and k_{-2} (also k_{-4}) increase when the receptor is being filled. It is noteworthy that, for instance, the increases in K_2 values can be 10 orders of magnitude when the occupancy of the receptor passes from 0 to 80%, or 8 orders of magnitude in the case of K_4 (data obtained by simulation as indicated in legend to Figure 5). There also a linear dependence of log([RL]/[R*L]) upon the occupancy of the receptor expressed as the relationship *total binding/(maximum binding − total binding)* (data not shown).

The results obtained in association−dissociation experiments can be explained from the values stated in Table 1. Thus, in dissociation experiments carried out by displacement with nonlabeled ligand, the empty receptor is rapidly filled by the nonlabeled agonist; then practically all the free receptor is converted into the lower-affinity form (R), which interacts faster with the ligand. At the same time, R*L is slowly converted to RL. Thus, the dissociation from R*L is detected when the concentration of [^{3}H]R-PIA used in the association is low, but not when it is high. In the latter case, after association, R and RL are practically the only species present. In contrast, when dissociation is performed by dilution, the four possible species are detectable in the course of the experiment.

Predictions of the Cluster-Arranged Cooperative Model. Experimental data in Figures 1 and 2 can be accurately simulated using the parameters in Table 1 for the *cluster-arranged cooperative model*. Furthermore, the *cluster-arranged cooperative model* predicts some characteristics of the behavior displayed by heptaspanning membrane receptors. Below we report the predictions of the model related to differences in maximum binding obtained when two different ligands are used and to desensitization mechanisms.

From the results reported about A_1 adenosine receptors, it is interesting to note that equilibrium binding data obtained with different ligand or allosteric enhancers, when fitting to the *two independent receptors model*, yield variable values for R_{total}. Obviously, this is a strong indication that this model is unsatisfactory since R_{total} should not depend on the ligand used. Assuming the *cluster-arranged cooperative model*, a set of data was generated for different hypothetical ligands using the constant values shown in Table 1 and according to the following differential equations system:

$$\frac{dx_1}{dt} = (R_{total} - x_1 - x_2 - x_3)(L_{total} - x_1 - x_3)k_1 - x_1k_{-1}$$

$$\frac{dx_2}{dt} = (R_{total} - x_1 - x_2 - x_3)k_2 - x_2k_{-2} - x_2k_3(L_{total} - x_1 - x_3) + x_3k_{-3}$$

$$\frac{dx_3}{dt} = x_2k_3(L_{total} - x_1 - x_3) - x_3k_{-3}$$

$$k_2 = k_{20}(1/Y)^{[(x_1+x_3)(f-1)]/(R_{total}-x_1-x_3)}$$

$$k_{-2} = k_{-20}(1/Y)^{[(x_1+x_3)f]/(R_{total}-x_1-x_3)}$$

where x_1, x_2, and x_3 stand for RL, R* and R*L, respectively.

A different value of Y (between 0.025 and 1) was assigned to each ligand for generating data, which were fitted to the

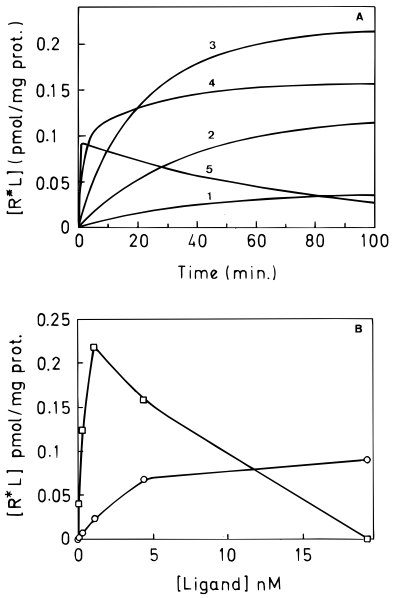

FIGURE 5: Simulation of the time course of appearance of [R*L]. Simulations were performed using the differential equations for the species of the *cluster-arranged cooperative model* (Chart 2) as indicated under *Experimental Procedures*. (A) Time course of the appearance of R*L at the following [^{3}H]R-PIA concentrations (nM): curve 1 (0.09), curve 2 (0.33), curve 3 (1.11), curve 4 (4.38), and curve 5 (19.34). (B) Dependence upon the [^{3}H]R-PIA concentration of [R*L] at equilibrium (□) and at 1.9 min (○).

cluster-arranged cooperative model and to the *two independent receptors model*. The R_{total} values obtained with the *two independent receptors model* vary with the ligand assumed. As expected, the fit to the *cluster-arranged cooperative model* gives the same R_{total} for every ligand, and this is always higher or equal (when Y is near 1) than that obtained with the *two independent receptors model* (data not shown). This would explain that the change of ligands (agonists or antagonists) or the use of allosteric enhancers apparently modifies the maximum binding when the *two independent receptors model* is considered.

In an impressive contribution using transgenic mice, Bond et al. (1995) have recently studied the physiological effects of inverse agonists of the β_2-adrenoreceptor. According to the response that different agonists produce in atria overexpressed with the β_2-adrenoreceptor, the authors postulate that different agonists might affect the equilibrium between the two conformational forms of the receptor (also called R and R*). In terms of ligand binding, this hypothesis can be explained by our model by assuming that every ligand has his own behavior concerning the displacement of the equilibrium between R and R*. This different behavior, as noted above, can be qualified by different Y values. In this way, in kinetic binding measurements, there is no need to specify whether a ligand is an "inverse" agonist or not. This term can, of course, be useful in terms of signal transduction responses.

On the other hand, one consequence of the variation of k_2, k_{-2}, k_4, and k_{-4} with the occupancy of the receptor is that the concentration at equilibrium of the form R*L reaches a maximum at a concentration of ligand of approximately 1.1 nM and then decreases markedly (see Figure 5). When simulating the time course of appearance of R*L, it is shown for the higher ligand concentrations that the maximum of [R*L] is achieved at approximately 1.9 min whereas, afterward, its concentration at equilibrium would be almost zero (see Figure 5). If only R* is the form able to transmit signals, the amount of signal produced may depend upon [R*L]. Thus, it is possible that the transduction of the signal is a rather quick process that takes place in times where the concentration of the form that transmits signals (R*L) is approximately proportional to the total concentration of the ligand (time 1.9 min or less in the graph of Figure 5). At higher times, the concentration of R*L increases at relatively low concentrations, but it decreases at higher concentrations. Actually, at high ligand concentrations, the receptor is saturated in the RL form whereas [R*L] tends to zero and thus desensitization occurs. In this way, ligand-induced desensitization would come as a consequence of the kinetic process of binding, thus explaining why it occurs at high ligand concentrations. As presented, this desensitization mechanism can be of general validity for membrane receptors.

ACKNOWLEDGMENT

We are grateful to Robin Rycroft from the Servei d'Assessorament Lingüístic de la Universitat de Barcelona for the excellent technical assistance in the preparation of the manuscript. We thank Dr. Juan José Novoa from the department of Physical Chemistry of the Universitat de Barcelona for computer technical assistance.

REFERENCES

Allende, G., Franco, R., Mallol, J., Lluis, C., & Canela, E. I. (1991) *Biochem. Biophys. Res. Commun. 181*, 213−218.

Bond, R. A., Left, P., Johnson, T. D., Milano, C. A., Rockman, H. A., McMinn, T. R., Apparsundaram, S., Hyek, M. F., Kenakin, T. P., Allen, L. F., & Lefkowitz, R. J. (1995) *Nature 374*, 272−276.

Bruns, R. F., & Fergus, J. H. (1990) *Mol. Pharmacol. 38*, 939−949.

Canela, E. I. (1984) *Int. J. Biomed. Comput. 15*, 121−130.

Canela, E. I., & Franco, R. (1986) *Biochem. J. 233*, 599−605.

Canela, E. I., Canela, M. A., & López-Cabrera, A. (1990) *Int. J. Biomed. Comput. 25*, 7−20.

Casadó, V., Cantí, C., Mallol, J., Canela, E. I., Lluis, C., & Franco, R. (1990a) *J. Neurosci. Res. 26*, 461−473.

Casadó, V., Martí, T., Franco, R., Lluis, C., Mallol, J., & Canela, E. I. (1990b) *Anal. Biochem. 184*, 117−123.

Casadó, V., Mallol, J., Lluis, C., Franco, R., & Canela, E. I. (1991a) *J. Neurochem. 57*, 1623−1629.

Casadó, V., Mallol, J., Lluis, C., Canela, E. I., & Franco, R. (1991b) *J. Cell. Biochem. 47*, 278−288.

Casadó, V., Mallol, J., Canela, E. I., Lluis, C., & Franco, R. (1991c) *FEBS Lett. 286*, 221−224.

Casadó, V., Mallol, J., Canela, E. I., Franco, R., & Lluis, C. (1992) *Eur. J. Pharmacol., Mol. Pharmacol. Sect. 225*, 7−14.

Casadó, V., Allende, G., Mallol, J., Franco, R., Lluis, C., & Canela, E. I. (1993) *J. Pharmacol. Exp. Ther. 266*, 1463−1474.

Ciruela, F., Casadó, V., Mallol, J., Canela, E. I., Lluis, C., & Franco, R. (1995) *J. Neurosci. Res. 42*, 818−828.

De Lean, A., Stadel, J. M., & Lefkowitz, R. J. (1980) *J. Biol. Chem. 255*, 7108−7117.

De Meyts, P., van Obberghen, E., & Roth, J. (1978) *Nature 273*, 504−509.

Donner, D. B. (1980) *Biochemistry 19*, 3300−3306.

Guijarro, L., Courineau, A., Calvo, J. R., & Laburthe, M. (1989) *Regul. Pept. 25*, 37−50.

Klotz, K. N., Lohse, M. J., & Schwabe, U. (1986) *J. Neurochem. 46*, 1528−1534.

Levitzki, A. (1981) *Nature 289*, 442−443.

Linden, J. (1991) in *Adenosine in the nervous system* (Stone, T., Ed.) pp 103−108, Academic Press, New York.

Lohse, M. J., Lenschow, V., & Schwabe, U. (1984) *Mol. Pharmacol. 26*, 1−9.

López-Cabrera, A., Cabré, F., Franco, R., & Canela, E. I. (1988) *Int. J. Biomed. Comput. 23*, 9−20.

Lowry, O. H., Rosebrough, N. J., Farr, A. L., & Randall, R. J. (1951) *J. Biol. Chem. 193*, 265−275.

Manger, J. P., Vassent, G., & Bockaert, J. (1981) *FEBS Lett. 127*, 267−272.

Munson, P. J., & Rodbard, D. (1980) *Anal. Biochem. 107*, 220−239.

Neubig, R. R., Gantzos, R. D., & Thomsen, W. J. (1988) *Biochemistry 27*, 2374−2384.

Samama, P., Cotecchia, S., Costa, T., & Lefkowitz, R. J. (1993) *J. Biol. Chem. 268*, 4625−4636.

Sibley, D. R., DeLean, A., & Greese, I. (1982) *J. Biol. Chem. 257*, 6351−6362.

Wells, J. A. (1994) *Curr. Opin. Cell. Biol. 6*, 163−173.

BI952415G